Journal of Magnetic Resonance 209 (2011) 47–52

Contents lists available at ScienceDirect

Journal of Magnetic Resonance

journal homepage: www.elsevier.com/locate/jmr

Combining one-dimensional stray-field micro-imaging with mechanical field-cycling NMR: A new spectrometer design

M. Ditter [a,*], H. Stork [a,1], B. Schuster [a,b], F. Fujara [a]

[a] Institut für Festkörperphysik, TU Darmstadt, Hochschulstraße 6, 64289 Darmstadt, Germany
[b] GSI Helmholtzzentrum für Schwerionenforschung GmbH, 64291 Darmstadt, Germany

ARTICLE INFO

Article history:
Received 16 November 2010
Revised 28 December 2010
Available online 31 December 2010

Keywords:
FC-NMR
NMR stray-field micro-imaging
Spin–lattice relaxation dispersion in LiF

ABSTRACT

A new spectrometer design combining stray-field micro-imaging with mechanical field-cycling Nuclear Magnetic Resonance (FC-NMR), allowing for one dimensional spatial resolution in the order of 10 μm is described. The field-cycle is implemented by moving the probe in the stray-field of a superconducting gradient magnet. In this way a field range between 10 mT and 6.3 T is covered. The maximum transfer time is less than 5 s. Further, methods to correct for some of the imaging artefacts found in previous studies are implemented. The main objective of this design is a depth- and field-dependent investigation of the defect structure caused by heavy-ion irradiation of ionic crystals.

1. Introduction

Recently, one-dimensional NMR micro-imaging was introduced as a new tool to investigate the penetration dependent defect structure caused by heavy-ion irradiation of solids [1]. In [1] this method is demonstrated to be sensitive to radiation induced paramagnetic defects – mainly F-centres – which considerably shorten the spin–lattice relaxation time (T_1) of the target nuclei. Spatial resolution is achieved by applying a strong static field gradient perpendicular to the irradiated surface. With this method it has been possible to measure one-dimensional spin–lattice relaxation rate profiles with a resolution of the order of 10 μm.

In previous studies [1–3] we presented such NMR relaxation rate profiles measured on Lithium Fluoride (LiF) samples irradiated with various projectiles. Ionic crystals such as LiF are very sensitive for the creation of colour centres through electron excitation. Since at ambient temperature LiF is not amorphized by heavy-ion irradiation, the properties and distribution of these point defects can be conveniently studied with a multitude of techniques; for a review, see [4]. The essence of our NMR studies on LiF is illustrated in Fig. 1 (taken from [2]) which shows a typical relaxation rate profile of an irradiated sample. Three regions are distinguishable: region 1 within the ion penetration with strongly enhanced relaxation rate, a transition region 2 and region 3 which is located clearly beyond the ion range. In the latter the observed relaxation rates are still increased and only slowly decrease to the level found in non-irradiated crystals. The strength of this effect was found to depend strongly on projectile and fluence. We assigned the enhanced relaxation rate in region 3 to F-centres produced by secondary X-rays [3]. However, we still lack a quantitative understanding of this effect. In order to unravel the relaxation mechanism, field-dependent relaxation studies could be beneficial. Potentially, such measurements could provide information about defect types and distributions.

While for heavy projectiles the spin–lattice relaxation dispersion in region 1 can be examined by conventional field-cycling spectrometers without spatial resolution, region 3 with its position dependent relaxation does require such position dependent measurements.

In this article we present a further development of our micro-imaging setup [1] which renders spatially resolved field-cycling experiments possible. Further, this new design allows for a controlled alignment of the sample with respect to the field gradient direction. This is relevant for minimizing the width of the transition region 2 (Fig. 1). In this region the magnetization curves are not mono-exponential which is manifested by the increased error bars in Fig. 1. This is readily explained by a misalignment of the sample such that zones with different relaxation rates contribute to the signal. Also note that the increased error bar of the first data point in region 1 has a different cause. Here, the signal-to-noise ratio is reduced since at the edge of a misaligned sample only a smaller number of spins contributes to the signal. Finally, the long-time positioning accuracy is strongly increased as compared to the previous design, which had suffered from position drifts due to thermal expansion of several components.

* Corresponding author. Fax: +49 6151 16 3833.
E-mail address: Michael.Ditter@physik.tu-darmstadt.de (M. Ditter).
[1] Present address: Laboratoire National des Champs Magnétiques Intenses, 25 rue des Martyrs, 38042 Grenoble Cedex 9, France.

1090-7807/$ - see front matter © 2010 Elsevier Inc. All rights reserved.
doi:10.1016/j.jmr.2010.12.009

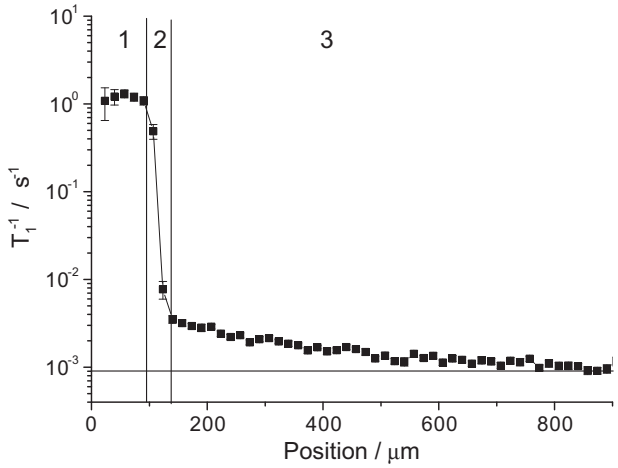

Fig. 1. ^{19}F-spin–lattice relaxation rate profile of a LiF crystal irradiated with 10^{12} ^{130}Xe ions/cm^2 (adopted from [2]). Three distinct regions are visible: region 1 within the ion range, a transition region 2 and region 3 clearly beyond the ion range. The distance between neighbouring data points is 17 µm. The profile was measured at a field of 3.74 T.

To our knowledge there is no similar device combining FC-NMR in solids with such a high spatial resolution. An extremely involved electronic FC magnet aiming for three-dimensional medical imaging has recently been published [5].

2. Spectrometer setup

2.1. Overview

In the design to be presented the probe is moved vertically in the stray-field of a superconducting 54-mm-bore magnet (Magnex Scientific Ltd., UK). The magnet is designed to provide a high static field gradient and was originally dedicated for static field gradient diffusometry [6]. The magnetic field profile along the vertical z-axis is shown in Fig. 2. Whereas between the two extremes the field isosurfaces are strongly curved in the stray-field their curvature becomes significantly smaller. At the marked position at about $z = 10$ cm (as well as at $z = -10$ cm) the isosurface is flat.

The positioning system consists of three distinct components (Fig. 3): a home built stage mounted on top of the magnet, the

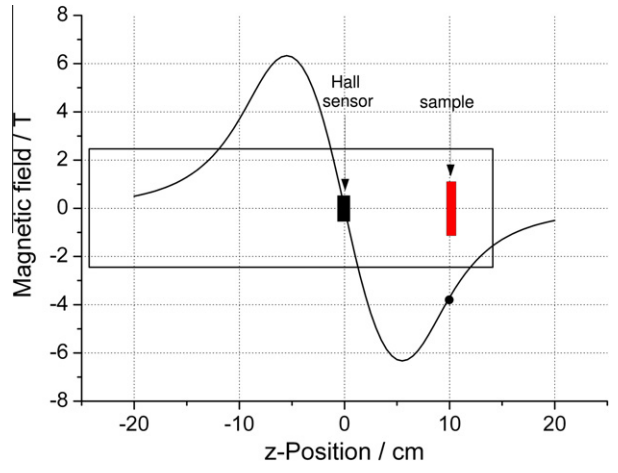

Fig. 2. Magnetic field profile. The NMR signal is detected at the marked position at approximately 10 cm. There, the magnetic field isosurface is flat. The probe (symbolized by the frame) is constructed such that the Hall sensor is at zero field when the sample is at the detection field.

necessary electronics with a programmable motion controller and a detachable probe. The stage includes a motor and an optical encoder to deliver feedback for the motion controller. Both are moving with the slide. Additionally to the encoder a Hall sensor is included in the probe to provide the controller with a reference point. In order to achieve an optimum spatial resolution, the surface of the sample has to be parallel to the magnetic field isosurfaces, i.e. perpendicular to the z-axis. Therefore the tilting of the sample is adjustable to compensate for mounting inaccuracies. The sample temperature can be controlled within the range from room temperature to 500 K.

The spectrometer is controlled by the home-written spectrometer control platform 'DArmstadt MAgnetic Resonance Instrument Software' (DAMARIS) – an extremely flexible, easily extendable open-source software [7].

2.2. Positioning stage

The main challenge was to construct a positioning system that is fast enough for field-cycling experiments while it still has to allow for a repositioning accuracy of about 1 µm. Conventional drives are either fast or accurate. Both demands are fulfilled by the HR-8 piezoelectric linear motor (Nanomotion Ltd., Israel). We use this motor in combination with a programmable DMC-2113 controller (Galil Motion Control, California) and a Mercury M1550S-40 optical differential digital quadrature encoder designed for a maximum speed of 7200 mm/s (MicroE Systems, Massachusetts). The encoder allows for a resolution of 0.5 µm. The HR-8 motor is capable of achieving a maximum speed of 250 mm/s and to deliver a maximum thrust of 32 N [8]. However, the achievable maximum speed depends on the thrust the motor has to deliver, while the resolution is limited by the used electronics and encoder. The sampling period of the controllers control loop is 125 µs limiting the response of the system.

The optical encoder and the motor are integrated in a home-built positioning stage. Both are mounted on a slide thereby moving with the probe. The motor operates against a ceramic coated steel drive strip on the opposite pillar. A type SSR-15 LM guide (THK CO., Ltd., Japan) is used to lead the slide. As pillars we chose two u-shaped aluminium profiles that provide the necessary stiffness under load.

To reduce the maximum load on the motor, gravity is compensated for by increasing pressure below the probe. This is done by inserting pressurized air at the bottom of the leading tube (Fig. 3). At the same time the generated airflow is used to cool the outside of the temperature controlled enclosure. The motor still has to overcome friction in the tube and the linear guide which limits its top speed to 140 mm/s. The encoder registers the reflected light from micro stripes on a glass scale, placed 20 µm apart. The resolution of 0.5 µm is achieved by 40-fold interpolation, with an interpolation accuracy of ±0.12 µm over any 20 µm movement. The long travel accuracy depends on the distance travelled from the reference point: ±3 µm up to 130 mm and ±5 µm up to 1 m [9]. Instead of a conventional mechanical reference point a Siemens KSY-10 Hall sensor is used as reference for encoder and controller. To ensure a high positional accuracy we average over 100 Hall sensor readings, which is carried out by the motion controller requiring 75 ms. The Hall sensor is connected with the sample by a 10 cm long quartz glass tube, such that the sensor is close to the magnetic field zero point while the sample is at the detection position, as illustrated in Fig. 2. This magnetic reference point is checked in each field-cycle just before the position is reached where the measurement takes place. Thus the probe has to be moved only for a few millimetres from the reference point, allowing to place the sample with an accuracy of about 1 µm. Thereby, also the drift of the sample position due to the thermal expansion of some components (probe, magnet cryostat, ...) is compensated for.

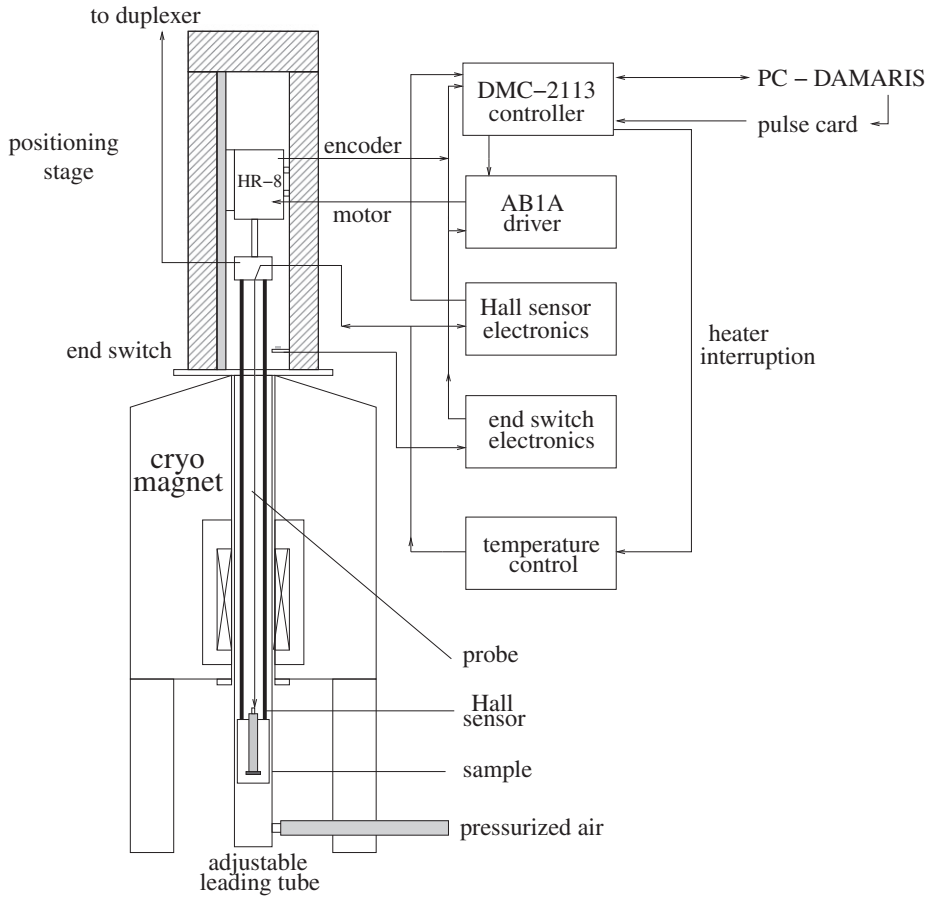

Fig. 3. Schematic overview of all components of the positioning system. The various elements are not up to scale.

The travel range of the stage is around 60 cm which corresponds to an available evolution field range from 0.01 T up to the maximum field of the magnet of 6.3 T. The transfer time t_{trans} between those fields is less than 5 s, which is shorter than typical spin–lattice relaxation times of most of the samples in region 3 – even at low fields. Thus the speed is generally sufficient to perform spin–lattice relaxation rate dispersion experiments in region 3.

2.3. The probe

The available space in the laboratory and the geometry of the magnet made it necessary to place the stage on top of the magnet. The desired position of the Hall sensor relative to the sample could be most easily realized by using the lower half of the magnetic field profile. As a consequence the probe has become rather long, about 1.4 m. Due to the motors limited thrust it has been designed to be as light as possible.

Wherever possible only non-conducting or poorly conducting materials are used in order to avoid eddy currents. The final design is presented in Fig. 4. The main body consists of six carbon fibre composite (CFK) tubes connected by Plexiglas rings. Three quartz glass tubes as well as the control rods for the tuning elements are running through these carbon fibre tubes. The quartz glass tubes connect the sample mount with the upper part of the probe. The tank-circuit is shielded by a 0.1 mm thick brass foil wrapped around the lower part of the probe. The two lowest Plexiglas rings

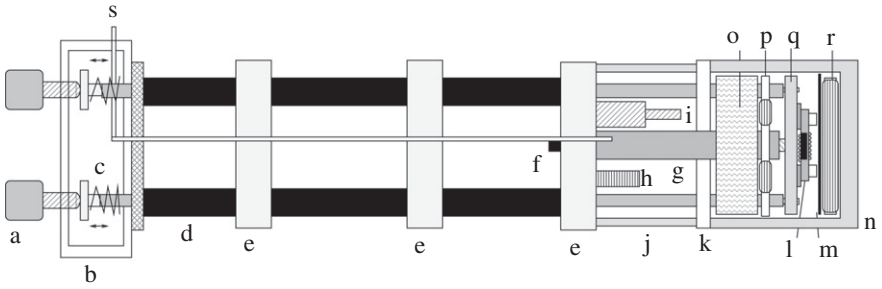

Fig. 4. The probe for spatially resolved mechanical field-cycling experiments: (a) adjustment screws, (b) aluminium casing with RF- and sensor connectors, (c) springs wrapped around the quartz glass tubes, (d) six CFK-tubes, (e) four Plexiglas stabilizers, the two lowest rings are also used to centre the probe in the guiding tube, (f) Hall sensor, (g) 10 mm quartz glass tube connecting the Hall sensor with the sample mount, (h) matching coil, (i) cylindrical tuning capacitor, (j) three brass pillars carrying the heater capsule, (k) Teflon base, (l) flat RF-coil wrapped around the sample, (m) isolating epoxy reinforced glass fibre layer, (n) lacquered Duratec cap, (o) ceramic wool, (p) lower heating coil, (q) sample mount, (r) upper heating coil, (s) RF-cable. The drawing is not up to scale.

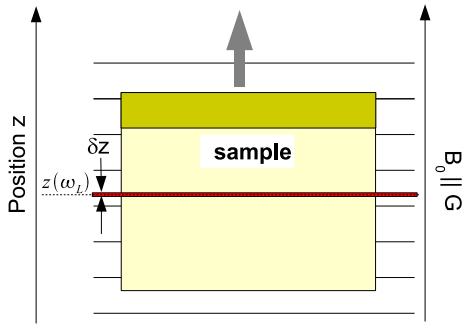

Fig. 5. Sample in a magnetic gradient field. The horizontal lines symbolize isolines of the magnetic field B_0. The nuclei are only in resonance in a thin excited slice at the fixed position $z(\omega_L)$ where the magnetic field corresponds to the central Larmor frequency. When the sample is moved, the exited slice "walks" across the sample. The darker area symbolizes region 1 within the ion range.

were especially fitted to the brass guiding tube to centre the probe; the other rings were built with more positional freedom.

The sample alignment is realized in two ways. First, the whole probe is moved inside the adjustable leading tube (Fig. 3), running through the magnet room temperature bore. Second, the sample mount in the probe is adjustable as well. It is placed on the three quartz glass tubes mentioned above, two of which can be moved with AJS Series high-precision adjustment screws (Newport Corporation, California) in order to tilt the sample. Quartz glass tubes were chosen to limit the impact of thermal expansion upon the distance between the optical encoder and the sample.

We use flat RF-coils wrapped around the sample embedded in a glass matrix. The benefits of flat RF-coils in static field gradient NMR are described in [10].

At the lower side of the probe a capsule is placed which can be heated. It contains the adjustable sample mount, two heating coils and one Pt-100 platinum resistor which is used to measure the temperature. The capsule, coated with lacquer for increasing the thermal isolation, is made from "Duratec" (Cape Siborit GmbH, Germany), an easily machinable ceramic material with a maximum service temperature of 1000 °C. Towards the room-temperature components an additional flexible layer of ceramic wool improves thermal isolation. All electrical leads for the coils and Pt-100 sensor are running through this layer. The two flat heating coils are wound on a Stenan substrate (WWS Keramik Neuhaus GmbH, Germany). Both coils are basically circular in shape, their diameter was chosen as large as possible to create a homogeneous temperature profile over the whole sample volume. The total heating power is 26 W, sufficient to heat the sample to temperatures up to 500 K. An Eurotherm 2216e PID controller is used to regulate the heating. Home-built electronics interrupt the current through the coils when the magnetization is read out.

3. Experimental

3.1. Samples

For the test measurements we chose LiF single crystals (Korth) partly already investigated in one of our previous studies [3]. Most irradiations were performed at the UNILAC linear accelerator of GSI Darmstadt. The crystals were exposed to 133 MeV ^{12}C, 1.78 GeV ^{208}Pb and, more recently, 644 MeV ^{58}Ni ions under normal beam incidence. In the crystal the heavy ions transfer energy to the target and slow down. The resulting dose profile depends on the projectile. In [3] a close relation between the dose profile and the spin–lattice relaxation rate has been reported. The projectile range, the mean range of the ions calculated with the TRIM code [11], is well defined within a typical straggling length of 3 μm, only. The respective projectile range was 245 ± 9.48, 76 ± 2.01 and 96 ± 3.16 μm. In addition, one sample was irradiated with 41.37 GeV ^{197}Au ions at the heavy-ion synchrotron SIS at GSI (range 4.83 mm [11]).

3.2. Measuring procedure

In order to implement FC we modified the stray-field imaging method described in detail in [1]. The field-cycle is presented in Fig. 6. First, a well defined initial state is created by applying a saturation comb in the detection field B_d. Then – in order to increase the signal-to-noise ratio for low evolution fields – the sample can be pre-polarized at B_{pol} = 6.3 T for a fixed period t_{pol}. After this initial preparation the sample is moved (within t_{trans}) to the evolution field B_{ev} where it stays for a variable time t_{ev}. In the stray-field, where gradients are lower, B_{ev} can be regarded as quasi-uniform over the entire sample volume in the context of relaxation. The

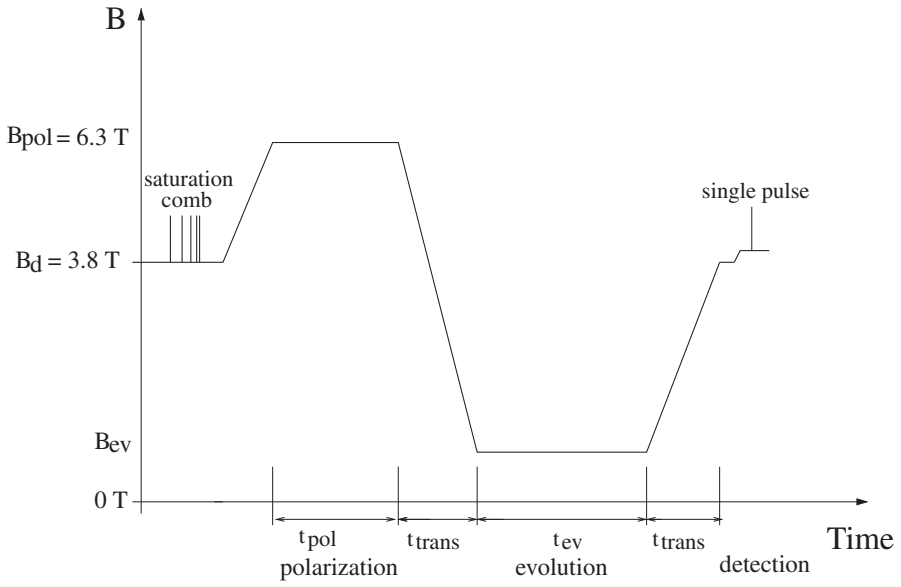

Fig. 6. Field-cycle, see text for detailed explanation. (*Note*: for high evolution fields the polarizing period can be skipped.)

change of the field strength is typically in the order of 2% over a 1 mm thick sample.

Before transferring the sample to the "detection" position the reference position, where the Hall sensor is near the field zero point, is checked after the "evolution" phase. Then the sample is moved to the detection field, thereby ensuring the high positional precision. The detection field is 3.8 T (corresponding to a Larmor frequency of 152.3 MHz for ^{19}F, the resonant nucleus in this study) with a field gradient of 74 T/m. In such a large field gradient not the whole sample is in resonance but only a thin excited slice with the thickness $\Delta z = \frac{1}{\gamma G t_p}$, where G is the field gradient, γ the gyromagnetic ratio and t_p is the pulse length. Since the applied pulses have a bandwidth of typically 20 kHz, only, Δz is in the micrometer range. The curvature of this excited slice follows that of the selected isosurface. Due to the narrow bandwidth free induction decays (FID), following single pulses, can be recorded for several slices of the sample during one field-cycle. In order to pass through slices the sample is moved such that the excited slice wanders over the sample (Fig. 5). This results in relaxation-weighted magnetization profiles (Fig. 7). The detection is done following an advanced sampling scheme, which is described in [1].

4. Test results

4.1. Field-cycling

The spectrometer was tested with a LiF single crystal, irradiated with a fluence of 3×10^{10} cm^{-2} ^{208}Pb and 10^{13} cm^{-2} ^{58}Ni ions. The ^{208}Pb irradiated sample is rectangular in shape, measuring $1 \times 1 \times 0.1$ cm^3. For this ^{19}F-NMR study RF-pulses with a length of 55 μs were used, corresponding to an excited slice width of 6 μm. T_1 was determined in the full field range, i.e. between 6.3 and 0.015 T. For each field 10–14 different waiting times t_{ev} were chosen. The ^{58}Ni irradiated sample is also rectangular in shape ($0.9 \times 0.53 \times 0.13$ cm^3). RF-pulses with a length of 47.5 μs were used, corresponding to an excited slice with a thickness of 7 μm. T_1 was determined in the field range between 6.3 and 0.125 T. Smaller B_{ev} were not accessible since at low evolution fields the (decreasing) relaxation times become shorter than the (increasing) transfer times. For each field 14 different waiting times were chosen. Below 2 T both crystals were pre-polarized at 6.3 T for 1800 s before being moved to the evolution field.

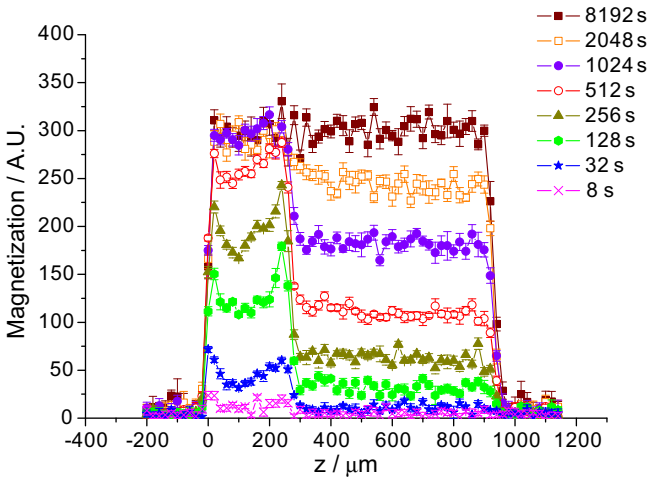

Fig. 7. Relaxation-weighted spatially resolved ^{19}F-magnetization profiles of a LiF crystal irradiated with 133-MeV ^{12}C ions of fluence 10^{11} cm^{-2}. During t_{ev}, the nuclear spin system recovers from saturation before the signal is read out.

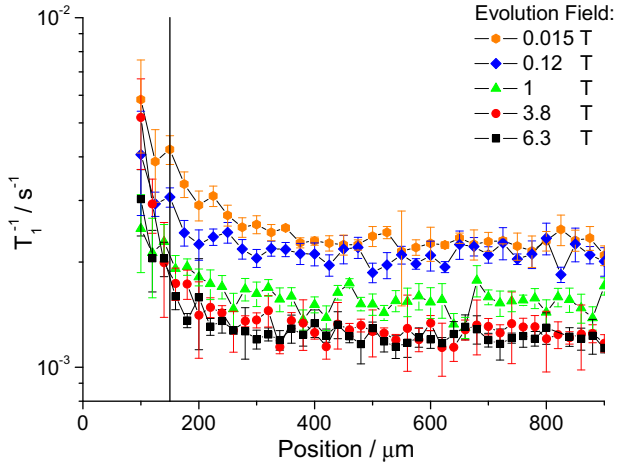

Fig. 8. ^{19}F spin–lattice relaxation rate dispersion of a LiF single crystal irradiated with 3×10^{10} ^{208}Pb ions per cm^2 in the region beyond the ion range. The vertical black line marks the end of the transition region 2. The distance between neighbouring data points is 25 μm (0.12, 0.015 T) and 20 μm (6.3, 3.8, 1 T).

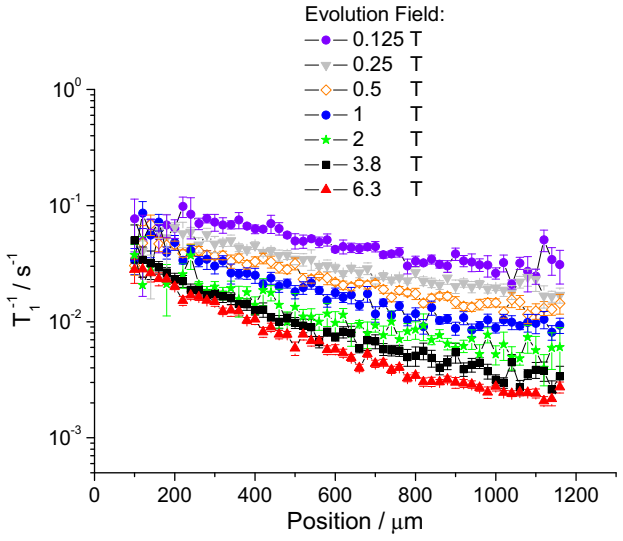

Fig. 9. LiF sample irradiated with 10^{13} ^{58}Ni ions per cm^2: ^{19}F spin–lattice relaxation rate dispersion in the region beyond the ion range. The distance between neighbouring data points is 20 μm.

In Figs. 8 and 9 the results for the two irradiated samples are shown in the region beyond the ion range. If we qualitatively compare the results obtained from both samples we see similarities but also several marked differences. In both samples the spin lattice relaxation rates generally increase with lower fields. In the ^{208}Pb irradiated sample the relaxation dispersion is much less pronounced than in the ^{58}Ni irradiated crystal. Further, its relaxation dispersion does hardly change over the examined part of the sample whereas it significantly changes in the ^{58}Ni irradiated sample. A more quantitative analysis of these and more data will be the topic of a separate publication.

4.2. Tilting

In previous experiments an approximately 50–100 μm wide transition zone between the regions within and beyond the ion range [2] was found. In this region the magnetization decay curves have multi-exponential contributions. Since the penetration of the

ions is well defined (typically straggling less than 3 μm [11]) it was previously not clear what causes these pronounced transition regions. It could only be suspected that they were caused by a poorly defined sample surface or sample misalignment in the magnetic field [2]. Thus, in addition to a better alignment, the samples are polished with sandpaper (1 μm grain size) to create better defined surfaces. In order to investigate the impact of both effects on spatial resolution the following experiments were performed: For the first experiment the LiF crystal irradiated at the SIS with the uniform spin–lattice relaxation time of 15 s without a polished surface was chosen in order to only examine the effect of a better alignment with the magnetic field. In Fig. 10 the flank of the optimally aligned sample is shown in comparison to that of same sample but misaligned. So far the flank width in the one dimensional magnetization profile could be reduced from 50 μm without optimized alignment, to 10–15 μm.

The second experiment was conducted on a LiF sample with polished surface. This sample was exposed to a fluence of

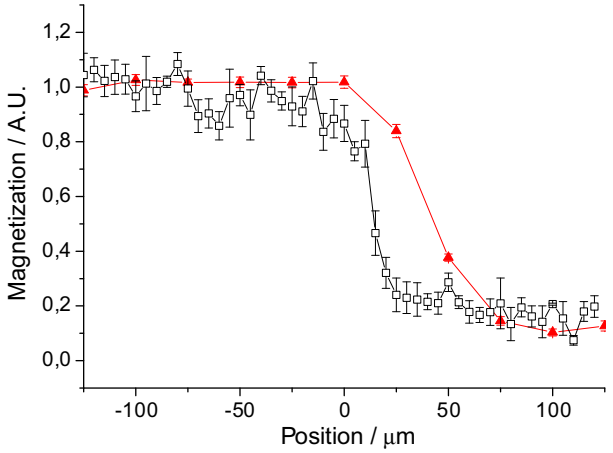

Fig. 10. ^{19}F magnetization profile of a LiF single crystal irradiated with 10^{11} ^{197}Au ions per cm^2 at the heavy-ion synchrotron SIS at GSI. The projectile energy was sufficiently high to penetrate the whole sample and to enhance the relaxation rate uniformly throughout the crystal. The edge of the crystal before (red) and after optimization (black) is shown. The final flank width is 10–15 μm, while the distance between neighbouring data points is 5 μm (black) and 25 μm (red). The zero position is set arbitrarily. (For interpretation of the references to colour in this figure legend, the reader is referred to the web version of this article.)

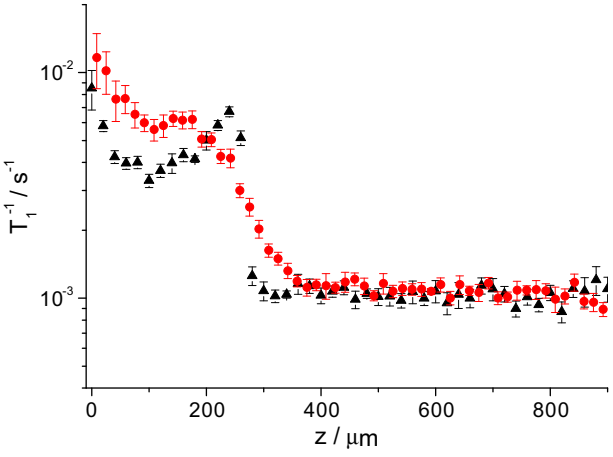

Fig. 11. ^{19}F spin–lattice relaxation rate profiles of a LiF sample irradiated with 10^{11} ^{12}C ions/cm^2. The red curve was measured without and the black curve after optimizing the alignment of the sample with respect to the magnetic field gradient. The distance between neighbouring data points is 20 μm (black) and 17 μm (red). (For interpretation of the references to colour in this figure legend, the reader is referred to the web version of this article.)

10^{11} cm^{-2} ^{12}C ions (straggling less than 10 μm [11]). Fig. 7 shows the relaxation-weighted magnetization and Fig. 11 the relaxation rate profiles of that sample. In Fig. 11 the red profile was measured without, the black one after optimizing the alignment of the crystal. The transition region 2 observed in all previous measurements has virtually disappeared while the rate increase at the end of the ion range (“Bragg peak”), so far only observed at higher fluences [3] where this effect is more pronounced, becomes visible. Note an increased relaxation rate close to the crystal surface which had not been recognized before. The reason for this increase is not clear but could be caused by a contamination of the beam with parasitic ions during irradiation.

These experiments suggest that the poor alignment of the sample was the dominant factor for the width of the observed transition regions in previous studies [1–3].

5. Conclusion

A setup for a spectrometer combining stray-field micro-imaging with mechanical field-cycling NMR was successfully implemented. This setup can be used to study relaxation effects position- and field-dependently. In addition, future micro-images will benefit from an enhanced spatial resolution thanks to optimized alignment of the irradiated crystals and improved long-time positioning stability. The appearance of the previously unexplained transition region 2 can now be attributed to sample misalignment.

First experiments have shown that spin lattice rate dispersion in region 3 (beyond the ion range) is indeed position dependent. Since at different distances from the ion range either the defect type or the defect distribution can be expected to change our experiments are believed to be of high relevance. Now it is necessary to conduct further systematic experiments and to deal with relaxation theory testing various defect (distribution) models.

Acknowledgments

We are grateful to the Deutsche Forschungsgemeinschaft (DFG) for funding this spectrometer as part of the project “Ortsaufgelöste NMR-Studien an schwerioneninduzierten Strahlenschäden in Fluoridkristallen” (Project No. FU 308/12).

References

[1] H. Stork, A. Hamburger, A. Gädke, F. Fujara, K. Schwartz, Spatially resolved characterization of heavy ion irradiated crystals using static field gradient nuclear magnetic resonance, J. Phys.: Condens. Matter 20 (2008) 275236.
[2] H. Stork, K.-P. Dinse, F. Fujara, A. Hamburger, P. Jakes, R. Neumann, B. Schuster, K. Schwartz, C. Trautman, Spatially resolved characterization of Xe ion irradiated LiF crystals using static field gradient NMR, J. Phys.: Condens. Matter 20 (2008) 465215.
[3] H. Stork, K.-P. Dinse, M. Ditter, F. Fujara, W. Masierak, R. Neumann, B. Schuster, K. Schwartz, C. Trautmann, Spatially resolved nuclear spin relaxation, electron spin relaxation and light absorption in swift heavy ion irradiated LiF crystals, J. Phys.: Condens. Matter 22 (2010) 185402.
[4] K. Schwartz, C. Trautmann, R. Neumann, Electronic excitations and heavy-ion-induced processes in ionic crystals, Nucl. Instrum. Methods Phys. Res., Sect. B 209 (2003) 73.
[5] K. Pine, G. Davies, D. Lurie, Field-cycling NMR relaxometry with spatial selection, Magn. Reson. Med.: Off. J. Soc. Magn. Reson. Med./Soc. Magn. Reson. Med. 63 (6) (2010) 1698.
[6] I. Chang, F. Fujara, B. Geil, G. Hinze, H. Sillescu, A. Tölle, New perspectives of NMR in ultrahigh static magnetic field gradients, J. Non-Cryst. Solids 172–174 (1994) 674.
[7] A. Gädke, M. Rosenstihl, C. Schmitt, H. Stork, N. Nestle, DAMARIS – a flexible and open software platform for NMR spectrometer control, Diffus. Fund. 5 (2007) 6.1.
[8] Nanomotion, HR8 Ultrasonic Motor User Manual, Yokneam, 2005. <www.nanomotion.com>.
[9] MicroE Systems, Mercury 1500 Digital Output Encoder Systems, Natick, 2006.
[10] H. Stork, A. Gädke, N. Nestle, F. Fujara, Flat RF coils in static field gradient nuclear magnetic resonance, J. Magn. Res. 200 (2009) 321.
[11] J.F. Ziegler, M.D. Ziegler, J.P. Biersack, The Stopping and Range of Ions in Matter, 2008. <http://www.srim.org>.